AD-A168 299

A 10-Gigahertz Space Power Combiner With Parasitic Injection Locking

by
Robert J. Dinger
David J. White
Research Department

and

Donald R. Bowling
Weapons Department

MARCH 1986

NAVAL WEAPONS CENTER
CHINA LAKE, CA 93555-6001

DTIC
SELECTE
MAY 3 0 1986

A

DTIC FILE COPY

86 5 29 008

Naval Weapons Center

FOREWORD

The research reported here on spatial power combining was supported by the Independent Exploratory Development (IED) program and was performed in fiscal year 1985. However, the concept had its genesis in the research on tightly coupled parasitic arrays that has been conducted over the past three years under sponsorship of the Office of Naval Research and the Independent Research program of the Naval Weapons Center. Support for this work by the IED program is continuing in fiscal year 1986.

M. Afendykiw has reviewed this report for technical accuracy.

It is a pleasure to acknowledge the following Naval Weapons Center personnel: C. F. Smith, A. R. Craddock, and D. J. Banks for their able assistance in fabricating and testing the array; T. W. Williams for calculations; and D. M. Kinman for helpful conversations.

AD-A168299

REPORT DOCUMENTATION PAGE

1a. REPORT SECURITY CLASSIFICATION UNCLASSIFIED		1b RESTRICTIVE MARKINGS		
2a. SECURITY CLASSIFICATION AUTHORITY		3. DISTRIBUTION / AVAILABILITY OF REPORT A Statement		
2b DECLASSIFICATION / DOWNGRADING SCHEDULE				
4. PERFORMING ORGANIZATION REPORT NUMBER(S) NWC TP 6704		5. MONITORING ORGANIZATION REPORT NUMBER(S)		
6a NAME OF PERFORMING ORGANIZATION Naval Weapons Center	6b. OFFICE SYMBOL *(If applicable)*	7a. NAME OF MONITORING ORGANIZATION		
6c. ADDRESS *(City, State, and ZIP Code)* China Lake, CA 93555-6001		7b. ADDRESS *(City, State, and ZIP Code)*		
8a. NAME OF FUNDING / SPONSORING ORGANIZATION Naval Weapons Center	8b. OFFICE SYMBOL *(If applicable)*	9. PROCUREMENT INSTRUMENT IDENTIFICATION NUMBER		

8c. ADDRESS *(City, State, and ZIP Code)* China Lake, CA 93555-6001	10. SOURCE OF FUNDING NUMBERS			
	PROGRAM ELEMENT NO. 62766N	PROJECT NO. 138865	TASK NO RZ66300	WORK UNIT ACCESSION NO.

11 TITLE *(Include Security Classification)*

A 10-Gigahertz Space Power Combiner With Parasitic Injection Locking (U)

12 PERSONAL AUTHOR(S)
Dinger, Robert J., White, David J., and Bowling, Donald R.

13a. TYPE OF REPORT Interim; Continuing	13b. TIME COVERED FROM Oct 84 TO Oct 85	14. DATE OF REPORT *(Year, Month, Day)* 1986, March	15. PAGE COUNT 36

16. SUPPLEMENTARY NOTATION

17.	COSATI CODES		18. SUBJECT TERMS *(Continue on reverse if necessary and identify by block number)*
FIELD	GROUP	SUB-GROUP	Power Combiners, IMPATT Diodes, Microstrip Antennas, Antenna Arrays
09	01		

19. ABSTRACT *(Continue on reverse if necessary and identify by block number)*

An array of three microstrip patch antennas, each connected by a matching network to an impact avalanche and transit time (IMPATT) diode, has been investigated. Coherent radiation from the array was obtained at 10.23 gigahertz by feeding only the center element with an injection-locking signal, which then appeared at the input to the other two elements by free-space mutual coupling. The three IMPATTs were successfully locked in this manner. A beamwidth of 38 degrees and sidelobe level of -10 decibels was achieved; this performance is consistent with the theory for coherent radiation from an array of this configuration. An efficiency of 90% was achieved, which is substantially greater than the efficiency that a cavity combiner and radiating elements can achieve. Scanning of the beam to 30 degrees from boresight was achieved; the scanning limit was shown to arise from excursions in the antenna impedance that caused the diodes to unlock. The bandwidth over which the three IMPATT diodes remained locked was measured to be 30 megahertz. This bandwidth is essentially the same as the bandwidth of an individual diode in its transformer.

20 DISTRIBUTION / AVAILABILITY OF ABSTRACT ☐ UNCLASSIFIED/UNLIMITED ☐ SAME AS RPT. ☒ DTIC USERS	21. ABSTRACT SECURITY CLASSIFICATION UNCLASSIFIED	
22a NAME OF RESPONSIBLE INDIVIDUAL Robert J. Dinger	22b TELEPHONE *(Include Area Code)* 619-939-1414	22c. OFFICE SYMBOL 3814

DD FORM 1473, 84 MAR

83 APR edition may be used until exhausted
All other editions are obsolete

SECURITY CLASSIFICATION OF THIS PAGE

CONTENTS

QUALITY INSPECTED 3

I. INTRODUCTION

One of the problems in the development of solid state transmitters is the design of efficient power combining structures. Individual solid state diodes generate relatively low radio frequency (RF) power levels (typically a few watts), and the outputs of many of these devices must be combined to achieve the tens or hundreds of watt levels required in radar systems and missile seekers.

Most combiner research has concentrated on closed structures, such as cavities or transmission lines (Reference 1); the diodes are coupled to this closed region, and the summed power is extracted at a single output port. If the power combiner output is ultimately radiated by an antenna array, then a closed combiner structure must be followed by a feed network for routing the signals to the array elements. Since the closed combining region and the feed network are efficiency-reducing sources of dissipative loss, for radiation applications it would be desirable to locate the diodes directly at the terminals of the array elements and combine the output power of the diodes "in free space," i.e., in the far field of the array. We refer to this type of array as a space power combiner.

This report describes a space power combiner consisting of an array of microstrip patch antennas, each element of which has a single impact avalanche and transit time (IMPATT) diode connected to its terminal (Figure 1). If allowed to free-run, each diode would oscillate with a frequency, power level, and RF phase that depend on the circuit impedance and specific diode conditions; the array would radiate incoherently. To force the IMPATTs to radiate coherently, an injection-locking signal must be supplied at the input to the diode. However, rather than piping an injection-locking signal individually to each diode, the scheme in Figure 1 requires only a single injection-locking signal applied to the center element. The injection-locking signal for the diodes at the terminals of the other elements appears by free-space mutual coupling between the elements.

At least three advantages accrue from this exploitation of the free-space coupling. First, the weight, bulk, and complication of transmission lines for an injection-locking signal for each element are eliminated. Second, a costly circulator is not required on each element for feeding the injection-locking signal. Third, the technique is better suited for planar integrated antennas because these extra components are not required.
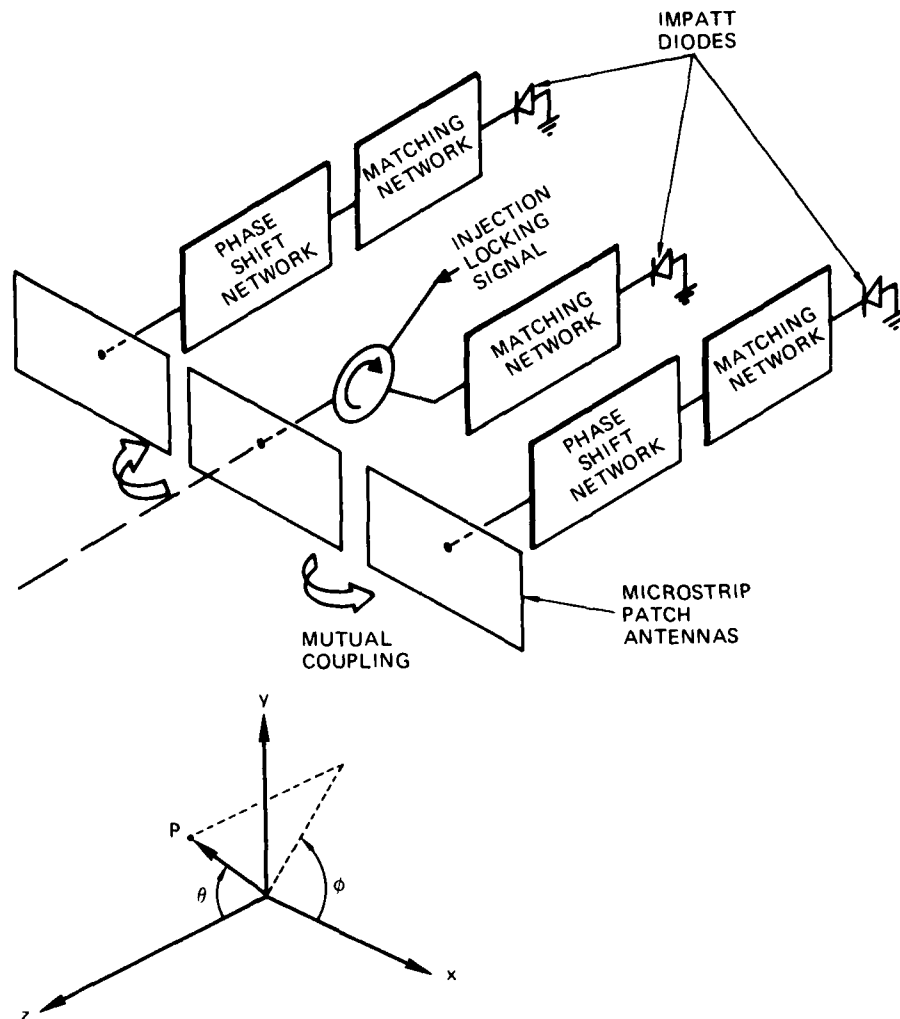
3

FIGURE 1.   Transmitting Array Using Parasitic Injection Locking.

Below, we present an analysis of the array (Section II), followed by a discussion of an experimental array operating at 10.2 gigahertz (Section III), and results obtained on this array (Section IV).   To summarize the results, we successfully obtained injection locking by mutual coupling and achieved an efficiency of 90% with this three-element array.   The features of the beam compare well with the features predicted by elementary array theory: The 3-decibel beamwidth is 38 degrees and the sidelobe level is 10 decibels.   Measurements of a preliminary nature on beam scanning show that the beam can be scanned to ±30 degrees from broadside with variable length shorts.

4

II. THEORY

Figure 2 is a diagram of a three-element array with an active one-port device terminating each element. The physical antenna terminals are labeled as Ports 1, 2, and 3; Port 4 is a terminal representing the power radiated to the far field of the array. Attached to each antenna terminal is a phase shifter P, a matching network M, a network T representing the impedance transformer that is integral to the diode mount, and the IMPATT diode. The phase shifter P supplies a phase shift of $+\phi$ in Arm 2 and $-\phi$ in Arm 3 to establish a phase gradient across the array aperture for beam steering. The matching network T is needed to transform the low impedance of the diode ($Z \approx -0.5 +3.0j$) to the $50+0j$ impedance of a connected transmission line. This matching network is integral to the diode mount and is discussed below. A priori, the matching network M should be viewed as possibly required, depending on whether the analysis shows that the impedance at the output of T should be further transformed to match the antenna impedance. The circulator in Arm 1 permits the injection-locking signal to be introduced.
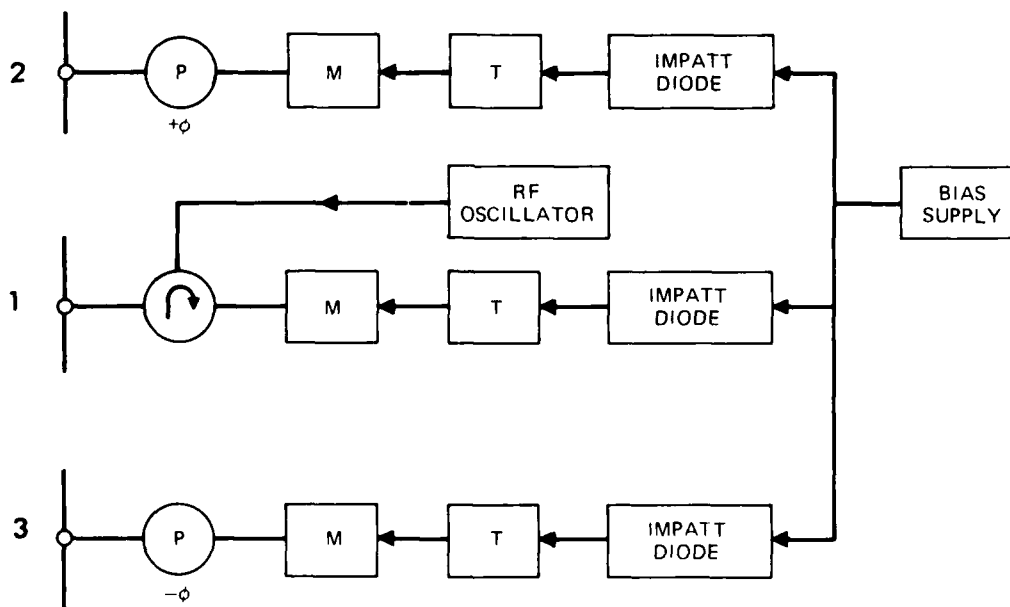

FIGURE 2. Block Diagram for Transmitting Array.

The goal of the analysis is to determine the impedance that the diodes, as transformed by T, must present to the array to ensure oscillation of the diodes in a desired mode. Hardware limitations in the realization of this impedance impact the bandwidth, maximum values of ϕ, and other array characteristics.

5

Figure 2 is redrawn in Figure 3. The network M has been removed, and the effect of the diode and its network T have been lumped together
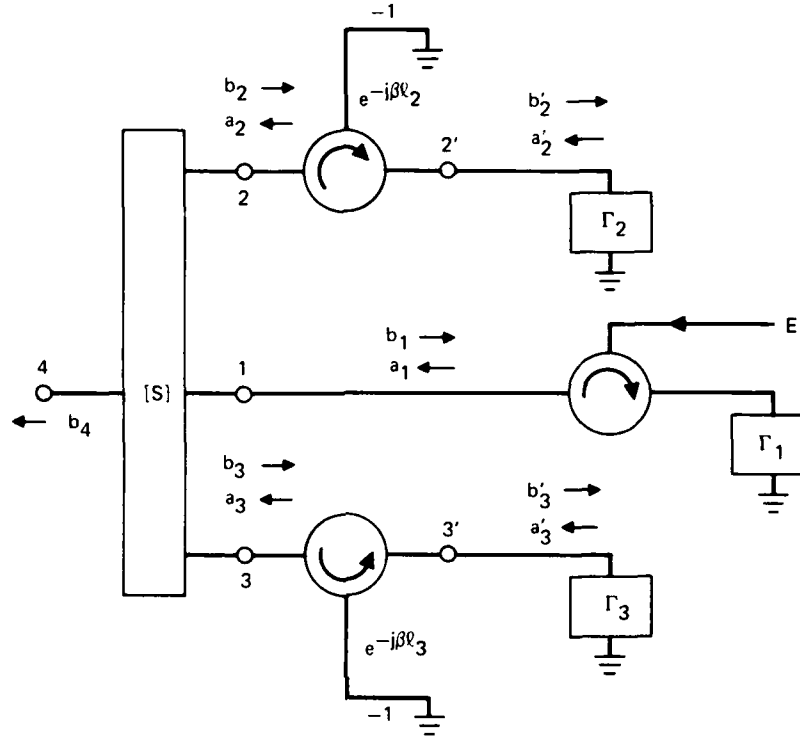

FIGURE 3. Array of Figure 2 With Simplifications Applied.

as a reflection coefficient Γ that terminates each arm. The scattering matrix [S] of the antenna array, assuming reciprocity and the appropriate symmetry, can be written:

$$[S] = \begin{bmatrix} S_{11} & S_{12} & S_{13} & S_{14} \\ S_{12} & S_0 & S_{23} & S_{24} \\ S_{13} & S_{23} & S_0 & S_{34} \\ S_{14} & S_{24} & S_{34} & S_{44} \end{bmatrix} \tag{1}$$

where $S_{22} = S_{33} = S_0$. Our primary interest is in the combination of a_i ($i = 1,2,3,4$) given by the vector $\vec{a} = (a_1, a_2{}', a_3{}', a_4)^T$ and in the corresponding combination of the b_i given by $\vec{b} = (b_1, b_2{}', b_3{}', b_4)^T$. We define [S'] as the scattering matrix that satisfies

6

$$\vec{b} = [S']\vec{a} \tag{2}$$

That is, $[S']$ includes the phase shifters, whereas $[S]$ does not. Assuming the lengths of the shorts on the reflection phase shifter circulators satisfy the condition $\ell_2 + \ell_3 = N\lambda/2$, the two-port scattering matrix for the phase shifter on Port 2 can be written as

$$\begin{pmatrix} a_2 \\ b_2' \end{pmatrix} = \begin{pmatrix} 0 & 1 \\ e^{-j\phi} & 0 \end{pmatrix} \begin{pmatrix} b_2 \\ a_2' \end{pmatrix} \tag{3}$$

and on Port 3 as

$$\begin{pmatrix} a_3 \\ b_3' \end{pmatrix} = \begin{pmatrix} 0 & 1 \\ e^{j\phi} & 0 \end{pmatrix} \begin{pmatrix} b_3 \\ a_3' \end{pmatrix} \tag{4}$$

where $\phi = 2\beta\ell$ ($\beta = 2\pi/\lambda$). Combining Equations 1 through 4, there results

$$\vec{b} = \begin{bmatrix} S_{11} & S_{12} & S_{13} & S_{14} \\ S_{12}e^{-j\phi} & S_0 e^{-j\phi} & S_{23}e^{-j\phi} & S_{24}e^{-j\phi} \\ S_{13}e^{j\phi} & S_{32}e^{j\phi} & S_0 e^{j\phi} & S_{34}e^{j\phi} \\ S_{14} & S_{24} & S_{34} & S_{44} \end{bmatrix} \vec{a} \tag{5}$$

We now substitute

$$\begin{aligned} a_1 &= \Gamma_1 E \\ a_2' &= \Gamma_2 b_2' \\ a_3' &= \Gamma_3 b_3' \end{aligned} \tag{6}$$

into Equation 5 and rearrange to get the following system of equations:

7

$$
\begin{bmatrix}
1 & - S_{12}\Gamma_2 & - S_{13}\Gamma_3 & 0 \\
0 & 1 - S_0\Gamma_2 e^{-j\phi} & - S_{23}\Gamma_3 e^{-j\phi} & 0 \\
0 & - S_{32}\Gamma_2 e^{j\phi} & 1 - S_0\Gamma_3 e^{j\phi} & 0 \\
0 & - S_{24}\Gamma_2 & - S_{34}\Gamma_3 & 1
\end{bmatrix}
\begin{bmatrix}
b_1 \\
b_2' \\
b_3' \\
b_4
\end{bmatrix}
$$

$$
=
\begin{bmatrix}
S_{11}\Gamma_1 E & + S_{14} a_4 \\
S_{12}\Gamma_1 e^{-j\phi} E & + S_{24} e^{-j\phi} a_4 \\
S_{13}\Gamma_1 e^{j\phi} E & + S_{34} e^{j\phi} a_4 \\
S_{14}\Gamma_1 E & + S_{44} a_4
\end{bmatrix}
\tag{7}
$$

We now assume that $a_4 = 0$, i.e., no external signal is incident on the array. Note that such an external signal, if present, would be essentially indistinguishable from the injection-locking signal E, since both occupy a similar location in the "driving" vector on the right-hand side of Equation 7.

Solving Equation 7 for b_4 by Cramer's rule yields

$$
b_4 = \Gamma_1 E \left[S_{14} + \frac{S_{24}S_{12}\Gamma_2(\gamma_3 + S_{23}e^{j\phi}\Gamma_3)e^{-j\phi}}{\gamma_2\gamma_3 - S_{23}^2\Gamma_2\Gamma_3} \right.
$$

$$
\left. + \frac{S_{34}S_{12}\Gamma_3(\gamma_2 + S_{23}e^{-j\phi}\Gamma_2)e^{j\phi}}{\gamma_2\gamma_3 - S_{23}^2\Gamma_2\Gamma_3} \right]
\tag{8}
$$

where $\gamma_2 = 1 - S_0 e^{-j\phi}\Gamma_2$ and $\gamma_3 = 1 - S_0 e^{j\phi}\Gamma_3$. Finally, by noting that in the far field of the array S_{14}, S_{24}, and S_{34} are related by

$$S_{24} = S_{14}e^{-j\beta\hat{r}\cdot d\hat{x}} \quad , \quad S_{34} = S_{14}e^{j\beta\hat{r}\cdot d\hat{x}} \tag{9}$$

where d is the separation between elements and $\hat{r}$ is the unit vector in the polar coordinate system of Figure 1 toward the observation point, Equation 8 can be written as

$$b_4 = S_{14}\Gamma_1 E \left[1 + \frac{S_{12}\Gamma_2(\gamma_3 + S_{23}e^{j\phi}\Gamma_3)}{\gamma_2\gamma_3 - S_{23}^2\Gamma_2\Gamma_3} e^{-j(\beta\hat{r}\cdot d\hat{x} + \phi)} \right.$$

$$\left. + \frac{S_{12}\Gamma_3(\gamma_2 + S_{23}e^{-j\phi}\Gamma_2)}{\gamma_2\gamma_3 - S_{23}^2\Gamma_2\Gamma_3} e^{j(\beta\hat{r}\cdot d\hat{x} + \phi)} \right] \tag{10}$$

This equation has several interesting features. Note that it is in the form of an antenna array factor: Each of the three terms is proportional to the element currents, multiplied by a phase factor accounting for the phase separation of the elements ($\beta\hat{r}\cdot d\hat{x}$) and the beam scan phase ϕ. The quantity b_4 represents the combined power appearing in the far field and is directly proportional to the injection-locking signal E. However, there can be a finite b_4 even when E = 0 if the denominators in terms two and three are zero, i.e., when

$$\gamma_2\gamma_3 - S_{23}^2\Gamma_2\Gamma_3 = 0 \tag{11}$$

This is the free run oscillation condition. It is a condition that should be met for best performance even when an injection-locking signal is applied, since Equation 10 implies that less injection signal is required for a given output as Equation 11 is more closely satisfied.

In practice, of course, a zero denominator in Equation 10 and the resulting "infinite" value of b_4 are not realized. The oscillation condition produces reflection coefficients greater than 1, and hence power generation, but the power generated by each diode saturates at some limiting value. A theory that accounts for this behavior and that thereby gives an estimate of power levels generated in the far field requires a nonlinear model of the diode. The inclusion of diode models in the theory is planned for a future paper.

For given values of the entries in [S], Equation 11 indicates that an unlimited number of combinations of Γ_2 and Γ_3 can satisfy the oscillation condition. In addition, the oscillation condition is a function of ϕ, implying that Z_{dT} must be changed as ϕ is changed. Although a ϕ-dependent T network in Figure 2 is conceivable, we did not incorporate this complication in the present experimental array. Our main goal is a well-formed broadside beam; symmetry thus requires $\Gamma_2 = \Gamma_3$, as evaluated at broadside. Setting $\phi = 0$ in Equation 11 and $\Gamma_2 = \Gamma_3 = \Gamma_0$ and solving for Γ_0 leads to

$$\Gamma_0^{\pm} = (S_0 \mp S_{23})^{-1} \tag{12}$$

The significance of two solutions corresponding to the two quadratic roots is not fully understood at this time, but the existence of such multiple solutions is fairly common in power combiner theory. (As will be seen below, the differences between the two solutions in Equation 12 are small for the experimental array.) Usually, one of the solutions is the correct cophasal combining mode, and the other solutions correspond to antiphasal modes that must be suppressed. However, it is not clear that such an interpretation is correct for this array. To emphasize: Γ_0 is the desired reflection coefficient that the IMPATT diode should present to the antenna array in order to satisfy the oscillation condition for $\phi = 0$.

For Γ_0 given by Equation 12, the oscillation condition will not be satisfied exactly as ϕ is made different from zero, i.e., as beam scanning is attempted. Defining the deviation from zero as Δ and manipulating the exponentials in Equation 11, we can write

$$\Delta = \Gamma_0^2(S_0^2 - S_{23}^2) - 2\Gamma_0 S_0 \cos \phi + 1 \tag{13}$$

Substituting Equation 12 into Equation 13 gives

$$\Delta^{\pm} = \frac{2S_0(1 - \cos \phi)}{S_0 \mp S_{23}} \tag{14}$$

as the deviation of the oscillation condition as a function of ϕ, assuming a symmetric broadside solution for Γ_0.

Next, these equations will be used with experimental values for [S].

III. EXPERIMENTAL ARRANGEMENT

A. ARRAY DESIGN

Figure 4 is a photograph of the experimental array. Microstrip patch elements were chosen for this array based on our earlier experience with closely coupled patch elements at 4 gigahertz (Reference 2).
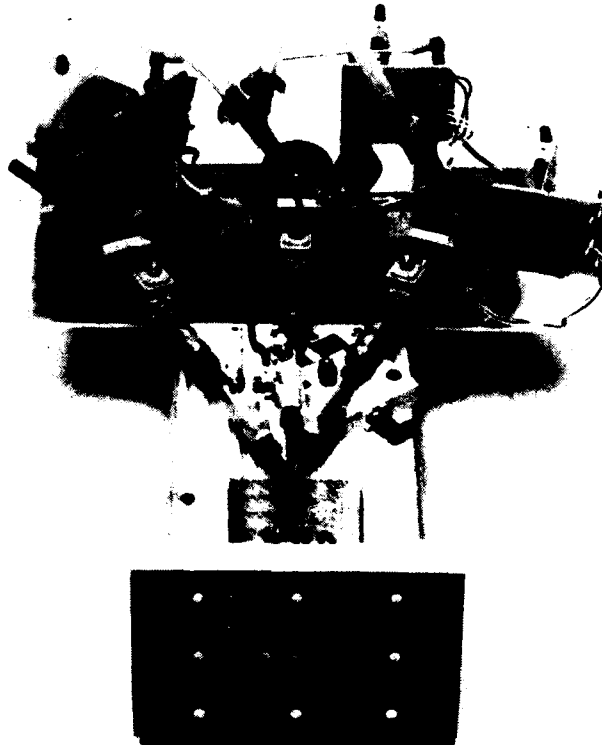

FIGURE 4. Experimental Array.

Table 1 lists the dimensions of the elements and gives some other characteristics of the array. The element sizes were derived using the standard equations based on the transmission line model of microstrip patch antennas (Reference 3). The feed position for each patch was computed using the same theory to yield an input resistance of 50 ohms.

TABLE 1. Array Properties.

Patch width × length, mm	8.66 × 12.0
Center-to-center separation, mm (wavelength)	14.0 (0.47)
Adjacent edge separation, mm (wavelength)	2.0 (0.067)
Substrate material	Duroid 5870
Substrate thickness, mm	0.79

The goal for mutual coupling between the center element and the two outside elements was about -13 decibels. This value was derived from earlier work with injection-locked IMPATT diodes that indicated the need for an injection signal level of about 100 milliwatts for successful injection locking. Assuming the center element radiates 2.0 watts (a conservative value for the diodes used with the array), a coupling of about -13 decibels is required. This is a relatively high coupling value for microstrip patch elements, and hence all possible steps were taken to maximize the coupling. The elements were spaced very close to each other, and colinear radiating edges were chosen because this configuration produces the tightest coupling (for closely spaced elements).

In Figure 5 we plot the return loss (S_{11}) and element coupling (S_{12} and S_{23}), as measured on a network analyzer. In Table 2 we list the coupling values, voltage standing wave ratio (VSWR), input
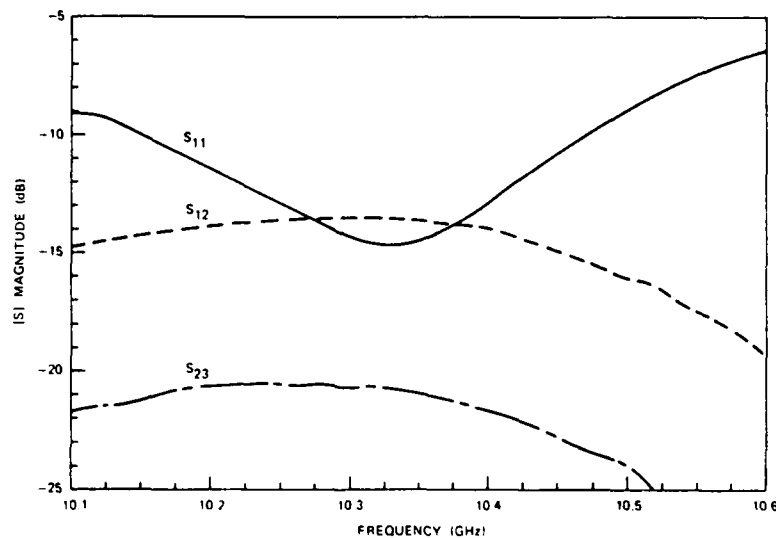

FIGURE 5. Return Loss and Interelement Couplings for Experimental Array.

12

impedance, and bandwidth extracted from these curves. The desired -13-decibel coupling was achieved, but the center frequency was 10.3 rather than 10.0 gigahertz.

TABLE 2. Measured Array Characteristics at Center Frequency = 10.33 Gigahertz.

[S] magnitude, dB	
S_{11}	-14.7
S_{22}	-14.5
S_{33}	-14.7
S_{12}	-13.7
S_{13}	-12.7
S_{23}	-20.7
VSWR	1.1:1
Input impedance, ohms	45.4 + j14
Bandwidth, MHz (2:1 VSWR)	300

B. IMPATT DIODE MOUNTS

Figure 6 shows a cutaway view of the IMPATT diode coaxial mount and transformer. An APC-7 connector whose characteristic impedance is 50 ohms joins the diode to an external circuit. The impedance transformation to the low impedance of the diode is accomplished using a single quarter-wave section of transmission line.

An analysis of the impedance transformer is given in the Appendix. To effect a match, the length ℓ_T and characteristic impedance Z_T of the impedance transforming section are adjusted. As shown in the Appendix, for an IMPATT with an impedance of $Z_d = R_d + jX_d$, the required values of ℓ_T and Z_T are given by

$$\ell_T = \frac{1}{\beta} \cos^{-1}\left(X_d \left\{ \frac{Z_0}{R_d[(R_d - Z_0)^2 + X_d^2]} \right\}^{1/2} \right) \tag{15}$$
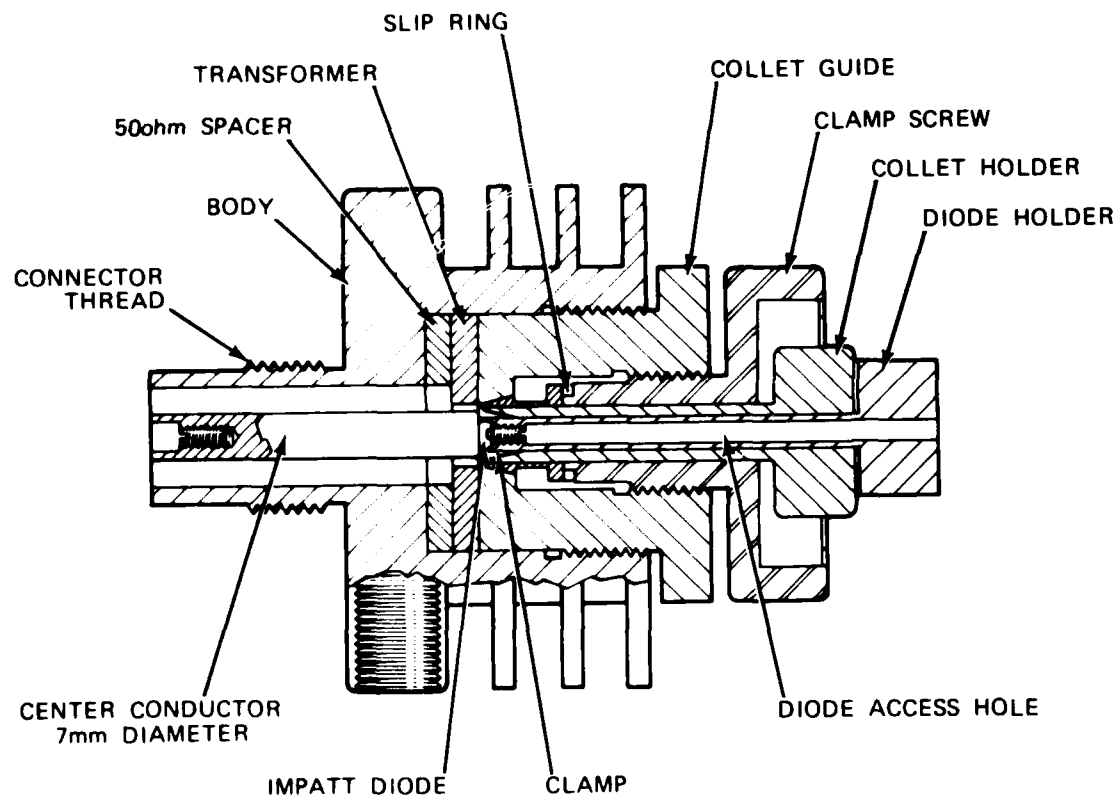
and

13

FIGURE 6. Cutaway View of IMPATT Diode Coaxial Mount.

$$Z_T = Z_0 \sin \beta \ell_T \left(\frac{R_d}{Z_0 - R_d \cos^2 \beta \ell_T} \right)^{1/2} \qquad (16)$$

where Z_0 = 50 ohms. Hence, for example, a diode impedance of Z_d = $-0.5 + j3.0$ ohms requires ℓ_T = 0.43 centimeters and Z_T = 3.98 ohms for a center frequency of 10.23 gigahertz (the operating center frequency used in the measurements). These values result in a transformed diode impedance of $-50 + j0$ ohms at the center frequency. The analysis neglects the small junction capacitances.

The impedance transforming properties of the transmission line section are considered further in the next section.

C. COMPARISON WITH IMPEDANCES DERIVED IN SECTION II

For Figure 7 the measured values of [S] were substituted into Equation 12, Γ_0 was converted into impedance by

$$Z^{\pm} = Z_0 \frac{1 + \Gamma_0^{\pm}}{1 - \Gamma_0^{\pm}} \tag{17}$$
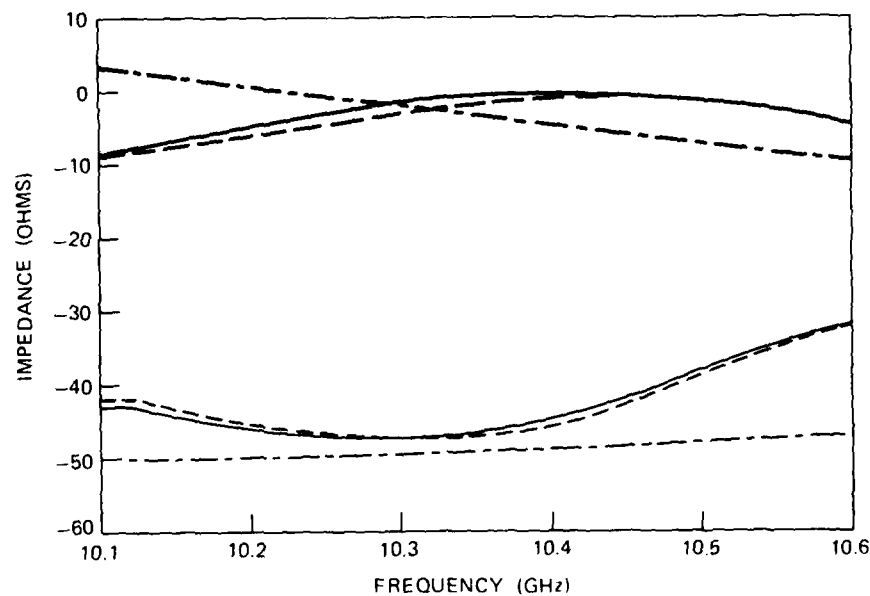
FIGURE 7. Comparison of Z (Equation 17) and Transformed Diode Impedance (Equation A-11). Heavy curves are reactance; lighter curves are resistance. Solid curves, Z^+; dashed curves, Z^-; dash-dot curves, Equation A-11.

and the impedance was plotted as a function of frequency. These curves represent the values of impedance that should be matched by the diode impedance, as transformed by T (Figure 2). Hence, for comparison, Figure 7 also shows this transformed impedance, as given by Equation A-11, for a typical diode with an impedance of $-0.5 + j3.0$ ohms at a frequency of 10.22 gigahertz. (As discussed in the Appendix, the slight frequency dependence of the diode reactance given by Equation A-12 is also included in this curve.) These curves indicate that a reasonably acceptable match is achieved between antenna array and diode over a frequency span of 10.1 to 10.3 gigahertz. For operation at the center frequency of 10.23 gigahertz used in the measurements, no additional matching network M (Figure 2) is needed.

15

D. EXPERIMENTAL CONFIGURATION

Figure 8 is a schematic diagram of the array, the diode mounts, and the diode drivers as set up in an anechoic chamber. The drivers pulse the IMPATT diodes with a 50% duty cycle square wave at a rate of 500 kilohertz. The power pattern of the array was measured by a power meter with an integration time much longer than the duty cycle of the diode drivers. The power meter was coupled to a standard gain rectangular horn antenna located 4.57 meters from the center of the array. Calibration of the chamber was accomplished using standard substitution techniques.
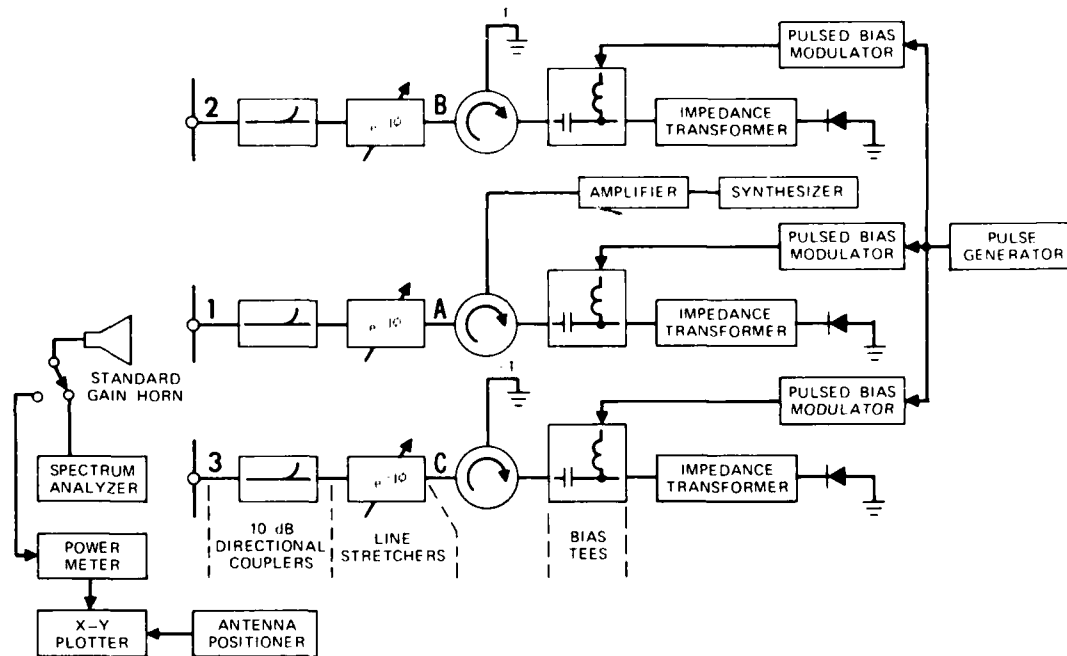
FIGURE 8. Diagram of Array and Test Apparatus.

E. PATTERN AND POWER CALIBRATION

A parameter of interest is the total radiated power P_r from which combiner far-field efficiency can be calculated. The total radiated power is given by

$$P_r = U_m \Omega_B \tag{18}$$

where U_m is the maximum radiation intensity and Ω_B is the beam solid angle given by

$$\Omega_B = \iint \left| F_{co}(\theta,\phi) \right|^2 \, d\Omega \tag{19}$$

The quantity $F_{co}(\theta,\phi)$ is the co-polarized field pattern (the ϕ direction in Figure 1) and $d\Omega = \sin\theta \, d\theta \, d\phi$ is the element of solid angle. The cross-polarized component has been neglected because of its relatively low value. The power density measured by the receiving horn is calculated from

$$U = \frac{P_o}{\Omega_o} = \frac{P_o r^2}{A_e} = \frac{4\pi r^2 P_o}{\lambda^2 G} \tag{20}$$

where P_o is the power meter reading, Ω_o is the solid angle subtended by the standard gain horn with gain G, r is the distance from the array under test to the horn, A_e is the effective receiving aperture of the horn, and λ is the wavelength. Substituting the values $G = 158$ (22 decibels), $r = 4.57$ meters, and $\lambda = 0.03$ meter gives

$$U = 1848 \, P_o \qquad \text{(watts/steradian)} \tag{21}$$

For a power meter reading P_o, Equation 21 gives the radiation intensity.

IV. EXPERIMENTAL RESULTS

A. FREE-RUNNING DIODES

The first step was to measure the frequency spectra of the IMPATT diodes individually as they were permitted to free run, i.e., with no injection-locking signal. Figure 9 shows the resulting spectra as measured at the far-field horn.

Two of the diodes oscillated with very nearly the same frequency (10.220 gigahertz), while the third oscillated at 10.227 gigahertz. We attempted to adjust the diodes to oscillate at 10.33 gigahertz, the center frequency of the array, but this frequency fell slightly outside the tuning range of the transformer section.

17
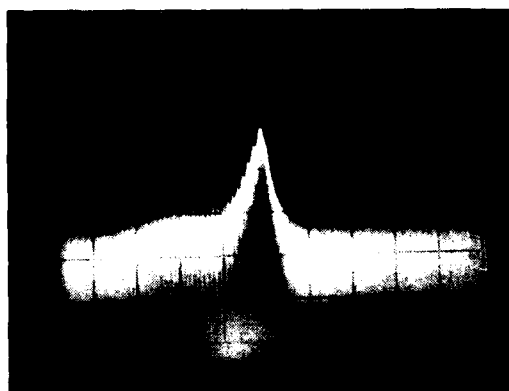
(a) Diode 1, center frequency = 10.22 gigahertz.
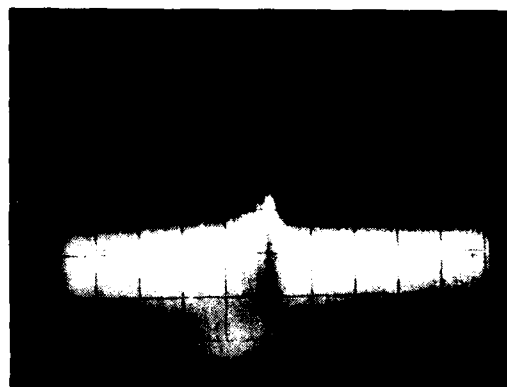
(b) Diode 2, center frequency = 10.227 gigahertz.

(c) Diode 3, center frequency = 10.22 gigahertz.

FIGURE 9. Spectra of Free-Running Diodes. Horizontal scale = 10 megahertz/division in all cases.

B. INJECTION LOCKING: BORESIGHT BEAM RESULTS

1. Patterns

To form a beam in the array boresight direction, the differential RF phase shift between the currents on the elements should be as small as possible. This requires that the electrical length of the transmission lines between the diodes and radiating elements must be equal. To set up the array for these conditions, a network analyzer was used to adjust the variable-length lines in Arms 2 and 3 for equal phase delay between points A and B, and between A and C (Figure 8).

An injection-locking signal was applied to the center element only, as shown in Figure 8, at a frequency of 10.230 gigahertz and with a power level of 0.55 watt. All diodes were driven at the same current level (690 milliamperes), and an H-plane pattern measurement (E_ϕ in the x-z plane of Figure 1) was made. Figure 10 shows the result. A beam with a 3-decibel width of 36 degrees was formed near broadside. The beam was squinted by 12 degrees from $\theta = 0$, indicating some small residual phase error between the elements. This phase error probably also accounts for the nonsymmetrical sidelobe structure.
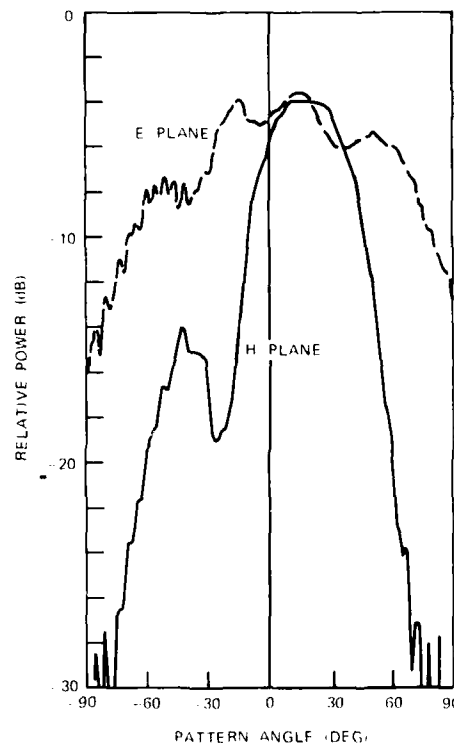
FIGURE 10. Measured Antenna Array Pattern. Drive current = 690 milliamperes. The E_ϕ component is shown.

The beamwidth and sidelobe level agree well with the predictions of simple array theory. The array factor for a three-element array with a phase center at Element 1 is given by

$$AF = \left| I_1 + I_2 e^{-j\beta d \sin \theta} + I_3 e^{j\beta d \sin \theta} \right| \qquad (22)$$

19

where the I_i (i = 1,2,3) are the relative current excitations. Equation 22, with d = 0.47λ and equal current excitation, is plotted in Figure 11. The 38-degree beamwidth and -10.0-decibel sidelobe level in this plot are in good agreement with the measured array values, perhaps fortuitous considering the assumption of noninteracting point sources implicit in Equation 22. However, the agreement is evidence that the three IMPATT diode sources are phased together and are radiating coherently.
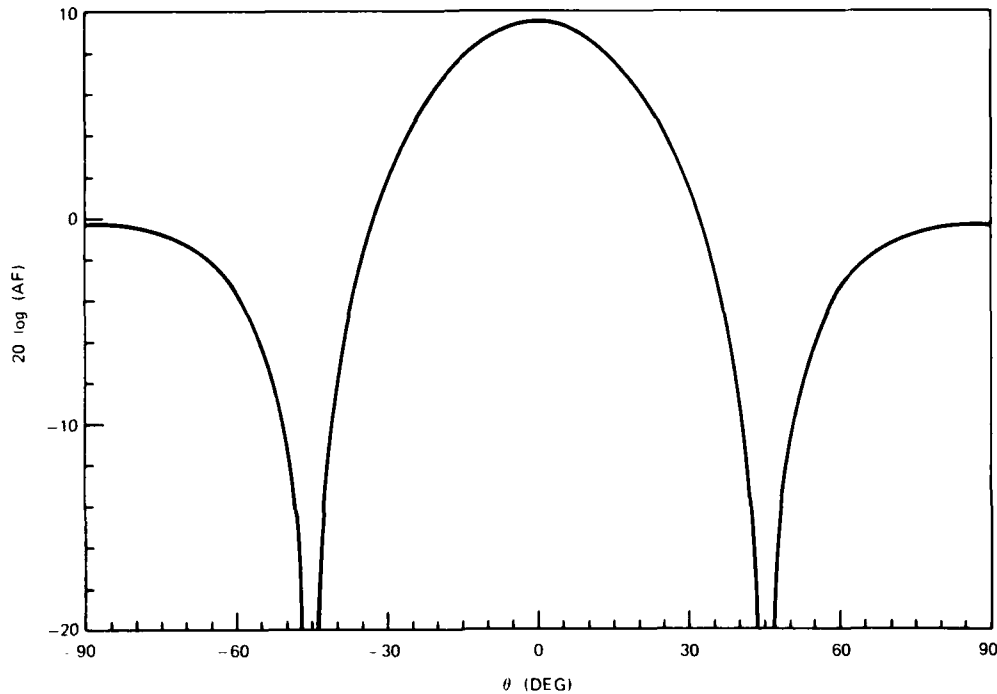

FIGURE 11. Plot of Theoretical Array Factor of Three-Element Array (Equation 25) With Uniform Excitation.

Figure 12 is conclusive evidence of source coherency; the spectrum of the signal received at the horn taken during the pattern measurement for Figure 10 is shown. A single peak results because of the injection locking.

The magnitude of the current excited in the antenna element can be controlled by the current supplied to the IMPATT diode by the driver. In Figure 13 we show a sequence of measured power patterns in which the current to Diodes 2 and 3 is progressively decreased below the current in Diode 1. Decreasing the current and therefore the power radiated by the outside elements is observed to lower the peak power (as expected) and to broaden the beamwidth. The trend is also predicted by the simple array theory, as shown in Figure 14. Table 3 is a summary of the experimental results in Figures 10 and 13.
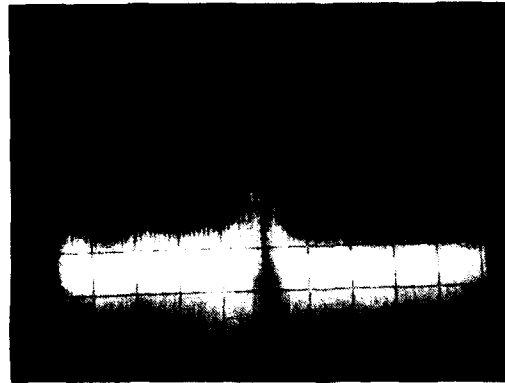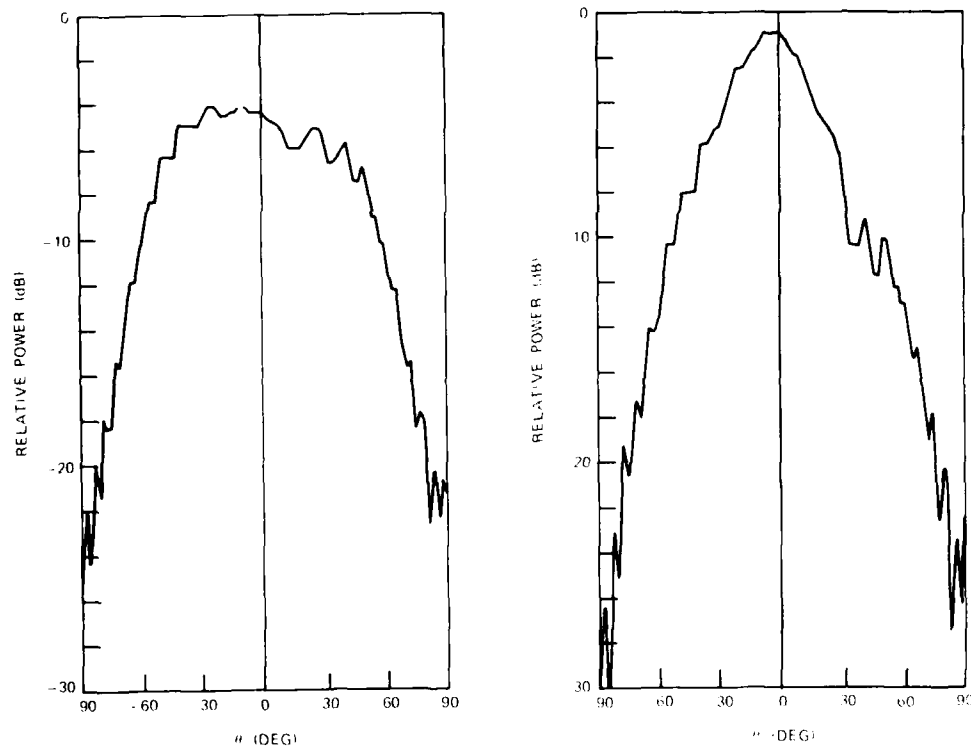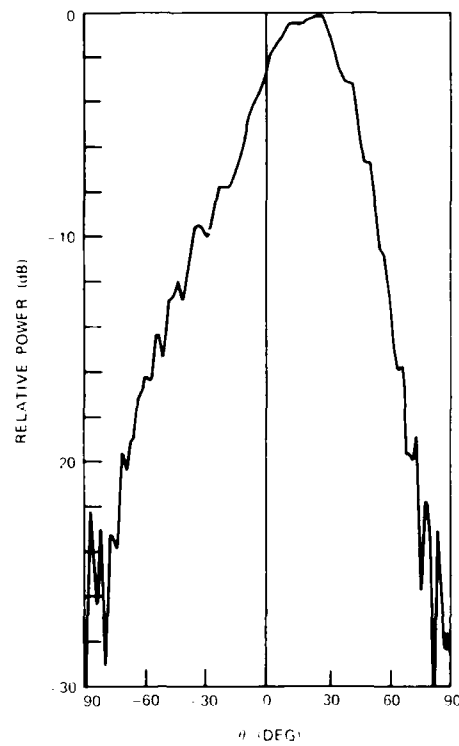
FIGURE 12. Spectrum of Transmitted Signal From Array. Center frequency = 10.23 gigahertz; horizontal scale = 10 megahertz/division.

(a) Drive current = 400 milliamperes.

(b) Drive current = 500 milliamperes.

FIGURE 13. Measured H-Plane Array Patterns.

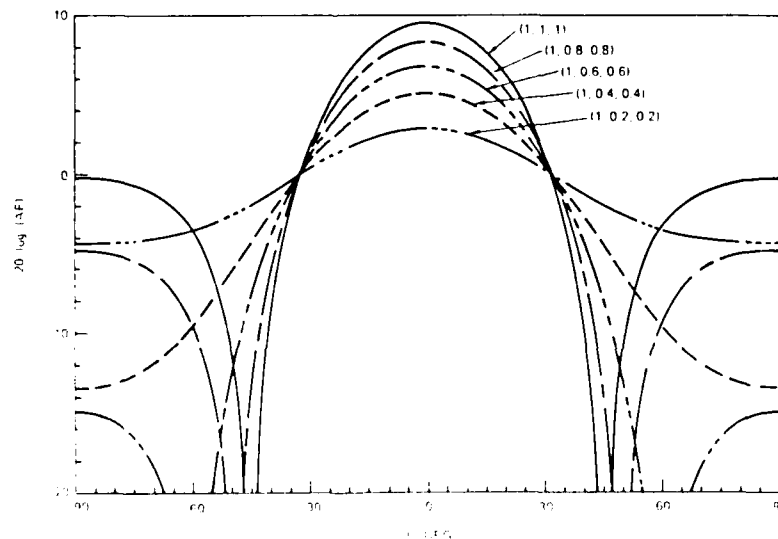(c) Drive current = 600 milli-
amperes.

FIGURE 13 (Contd.)

FIGURE 14. Plot of Theoretical Array Factor of
Three-Element Array (Equation 25) With Various
Relative Current Excitations. I_1, I_2, I_3 are given
in parentheses next to each curve.

22

TABLE 3. Summary of Boresight Beam Results
(Frequency = 10.230 Gigahertz).

Drive current, ma	400	500	600	690
3-dB Beamwidth, deg	100	45	41	38
Peak power, dBm	-0.7	2.40	3.3	5.9
Peak intensity, W/sr	1.57	3.21	6.10	7.19
Pattern figure number	13(a)	13(b)	13(c)	10

The cross-polarized pattern of the array in the H-plane (E_θ in the x-z plane of Figure 1) produced levels that were at least 20 decibels below the main beam level. An E-plane cut (E_θ in the y-z plane) has been included on Figure 10. We are not certain of the origin of the ripple in this pattern. Possibly it arises from diffraction from the edge of the ground plane or from chamber reflections. A smooth curve through the pattern ripple closely reproduces the E-plane pattern for a microstrip patch antenna (Reference 3).

2. Array Efficiency Measurement

We define the efficiency as

$$e = \frac{\text{total radiated power}}{\text{RF power generated by IMPATT diodes}} \times 100\% \qquad (23)$$

The total power generated by the IMPATT diodes was measured by disconnecting each diode at its circulator in Figure 8 and connecting a power meter. The measured values were 3.2, 3.0, and 3.7 watts, respectively, for Elements 1 through 3. The total RF power generated by the diodes is thus 9.9 watts. To compute the radiated power, the beam solid angle (Equation 19) must be computed from the measured data. The pattern in Figure 10 yields a beam solid angle of 1.25 steradians, where the measured E-plane cut has also been incorporated. We have neglected the contribution to the beam solid angle from the cross-polarized radiation because of its low magnitude.

The computed efficiency is e = 90.9%. The losses occur from at least two sources: (1) ohmic losses in the antenna elements, substrate, and feed transmission lines and (2) mismatch losses at the antenna terminals. This value of efficiency can be compared with the typical 70% value found for cavity combiners (Reference 1). However, the output of a cavity combiner must be routed over transmission lines and radiated into the far field by antenna elements, both of which

produce further losses. Hence, the far-field efficiency of a cascaded cavity combiner, feed network, and radiating element will compare even less favorably with the space-power combiner.
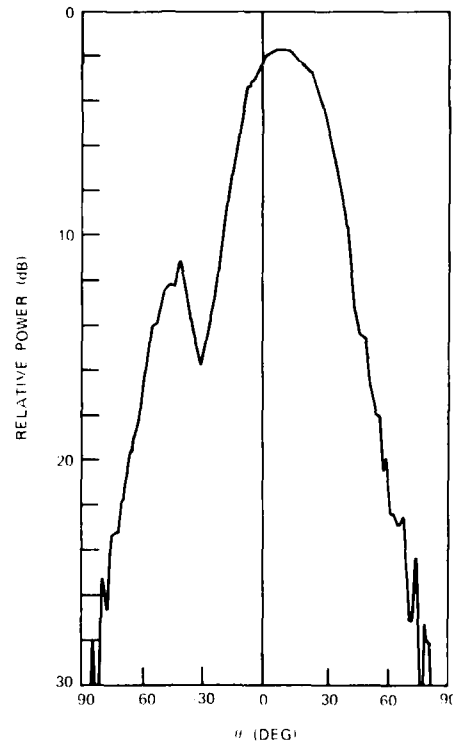
3. Bandwidth

The frequency sensitivity of the array is displayed in Figure 15. All diodes were driven at a current level of 690 milliamperes and the injection frequency was varied as shown. The breakup of the main beam below 10.22 gigahertz and above 10.25 gigahertz establishes the array locking bandwidth as approximately 30 megahertz.
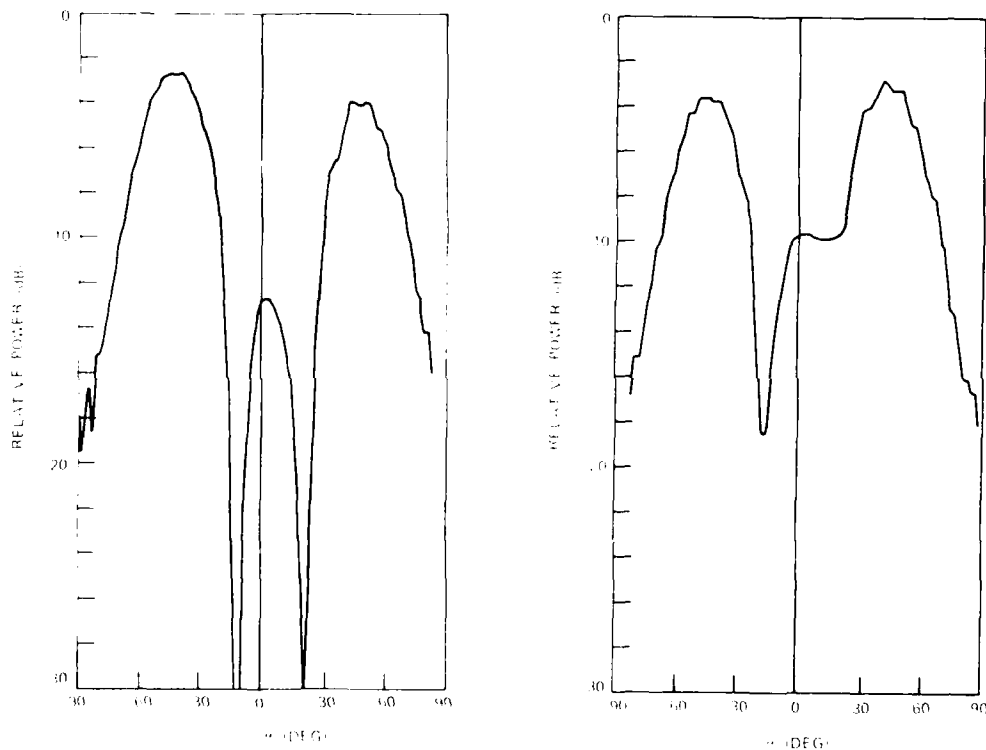
(a) Frequency = 10.20 gigahertz.   (b) Frequency = 10.21 gigahertz.

FIGURE 15. Change in Measured Antenna Array Pattern as a Function of Injection-Locking Frequency.

(c) Frequency = 10.25 gigahertz.

FIGURE 15. (Contd.)

The locking bandwidth of a single diode mounted in its transformer is of interest to identify the bandwidth-limiting factors. The locking bandwidth depends very much on the injection signal level. The approximate injection signal level at Elements 2 and 3 is given by (3.2 × 0.05) watts, or 160 milliwatts. The factor 0.05 arises from the -13-decibel coupling to the center element, and 3.2 watts is the measured injection signal level. The bandwidth of the IMPATT diodes mounted in their transformers but disconnected from the array was measured as 36 megahertz at an injection signal level of 160 milliwatts. The array impedance characteristic, as shown in Figure 7, possibly narrows the bandwidth slightly. However, since the array-locking bandwidth is essentially the same as the diode-plus-transformer bandwidth, we conclude that the bandwidth is limited by the diode characteristics and not by the antenna. If a diode bandwidth approaching the 300-megahertz bandwidth of the antenna array were achievable, the array would probably limit bandwidth.

C. INJECTION LOCKING: BEAM-SCANNING RESULTS

To move the beam from broadside, a constant interelement phase shift must be established. For the array configuration shown in Figure 8, this phase shift was provided by precision fixed shorts that were connected as shown to the circulators on Elements 2 and 3. These shorts shifted the phase of the injection-locking signal seen by the diode, thereby shifting the phase of the currents on the antenna elements. The disadvantage of this method is the transformation in antenna terminal impedance viewed by the IMPATT diode because of the extra line length of the shorts.

Beyond some electrical length, the impedance will be transformed out of the coherent locking range of the diodes. Or, from the point of view of Equation 14, the oscillation condition is not sufficiently satisfied.

This effect is shown in Figure 16. The value of $\Delta^{\pm}$ given by Equation 14 is plotted as a function of ϕ. The magnitude of $\Delta^{\pm}$ increases rapidly as ϕ is changed from zero. The exact effect that this change in $\Delta^{\pm}$ has on diode locking and beam scanning cannot be predicted without a specific model for the diode.
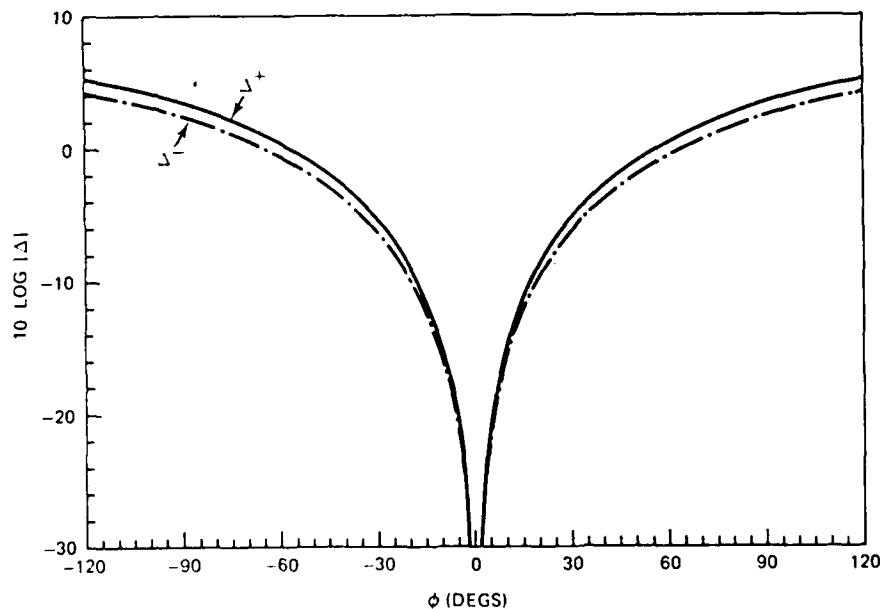

FIGURE 16. Dependence of $\Delta^{\pm}$ (Equation 14) on ϕ.

For experimental measurements, a network analyzer was first used to adjust the variable-length air lines in Figure 8 for zero differential phase shift between Elements 1 and 2, and 1 and 3, as was done for the boresight beam measurements. The resulting pattern is shown in Figure 17(a). The phase adjustment in this case is actually somewhat better than the adjustment obtained for the earlier measurements, since the beam is accurately aligned at 0 degrees.

A fixed-length short of electrical length -X degrees was then connected to the Arm 2 circulator, and a short of length +X degrees was connected to the Arm 3 circulator. Values for X of 30, 60, 90, and 120 degrees were used. The power patterns are shown in Figure 17, and Table 4 summarizes the results. For 30, 60, and (obstensibly) 90 degrees, the beam-steering angle shifts in the desired manner; the amount of shift is very close to the value predicted by elementary phased array theory, which states that the beam angle from boresight θ_b is given by

$$\theta_b = \sin^{-1}\left(-\frac{\phi}{\beta d}\right) \tag{24}$$

where ϕ is the interelement phase shift.

TABLE 4. Beam-Steering Results.

Interelement phase shift, deg	Main beam pointing angle, deg from boresight	
	Measured	From Equation 24
30	9	12.1
60	29	24.7
90	38	38.9
120	38	56.8

Actually, the good agreement at 90 degrees is only coincidental. At some phase shift value between 60 and 90 degrees, the impedance transformation produced by the electrical length of the shorts causes the IMPATT diodes to unlock. Measurements of the spectrum of the far field confirmed this. The patterns in Figures 17(d) and 17(e) are essentially the same because the array is not coherently radiating, and hence, the fixed shorts have no effect on the pattern.

27

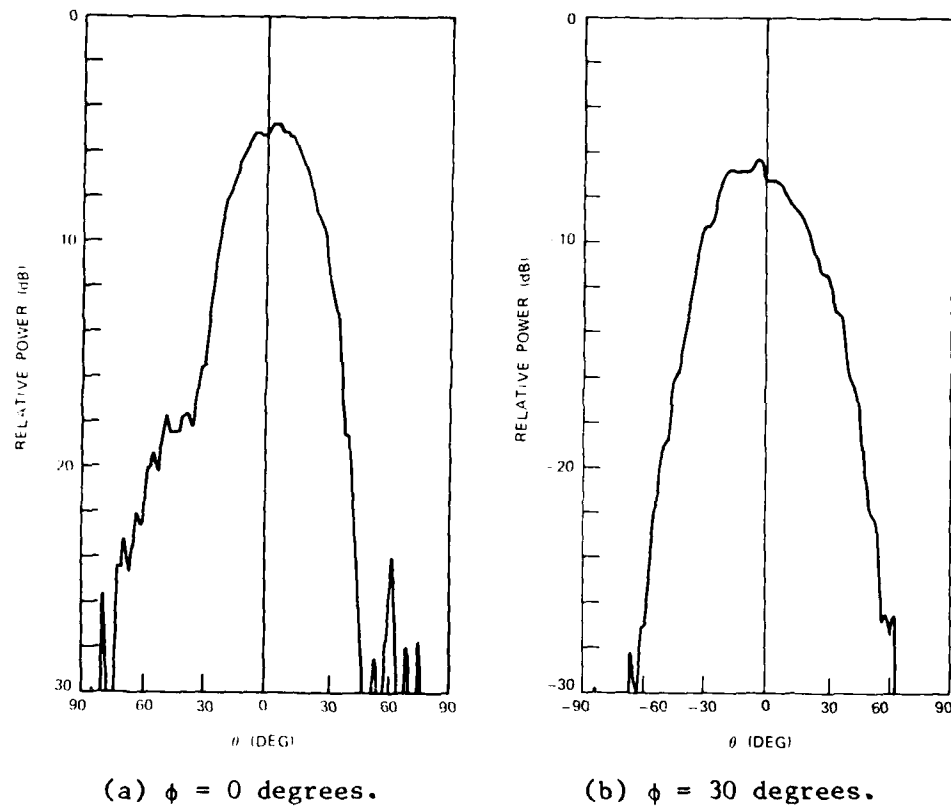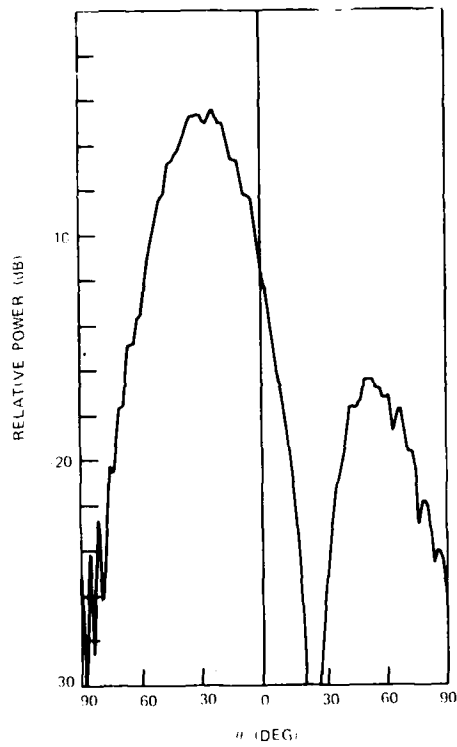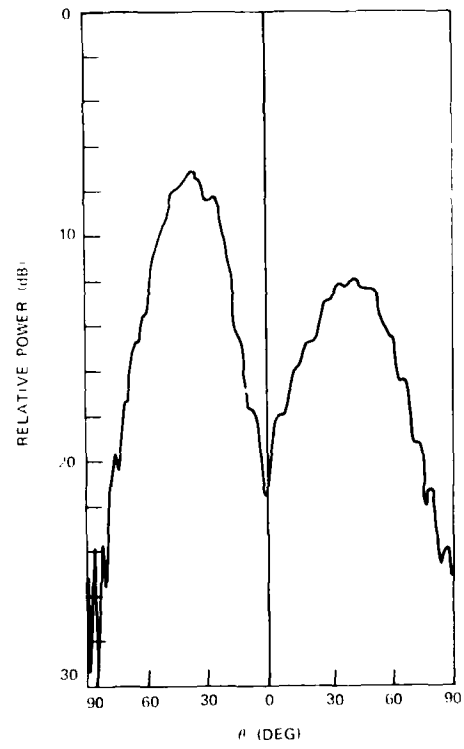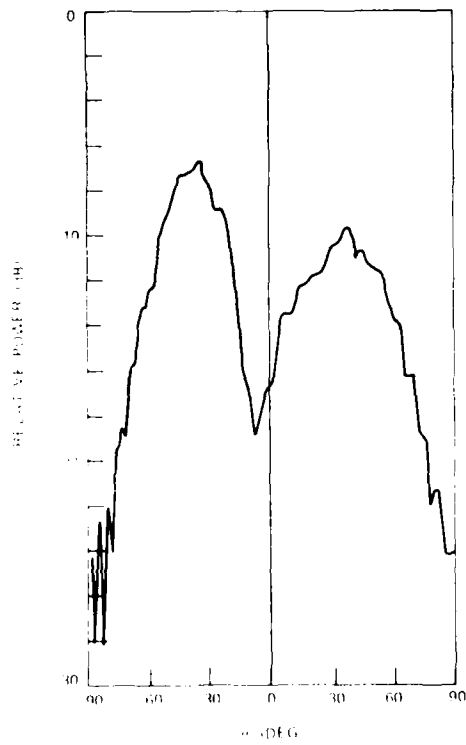(a) ϕ = 0 degrees.   (b) ϕ = 30 degrees.

FIGURE 17. Measured Antenna Array Patterns for Various Lengths
of Phase-Shifting Shorts.

(c)

(d)

(e)

(c) ϕ = 60 degrees.
(d) ϕ = 90 degrees.
(e) ϕ = 120 degrees.

FIGURE 17. (Contd.)

29

To summarize, variable-length shorts and circulators permit a limited beam-steering capability (±30 degrees). Greater excursions will require a phase-shifting technique that does not transform the impedance seen by the diodes.

V. CONCLUSIONS AND FUTURE WORK

An array of three microstrip patch antennas, each connected by a matching network to an impact avalanche and transit time (IMPATT) diode, has been investigated. Coherent radiation from the array was obtained at 10.23 gigahertz by feeding only the center element with an injection-locking signal, which then appeared at the input to the other two elements by free-space mutual coupling. The three IMPATTs were successfully locked in this manner. A beamwidth of 38 degrees and sidelobe level of -10 decibels was achieved; this performance is consistent with the theory for coherent radiation from an array of this configuration. An efficiency of 90% was achieved, which is substantially greater than the efficiency that a cavity combiner and radiating elements can achieve. Scanning of the beam to 30 degrees from boresight was achieved; the scanning limit was shown to arise from excursions in the antenna impedance that caused the diodes to unlock. The bandwidth over which the three IMPATT diodes remained locked was measured to be 30 megahertz. This bandwidth is essentially the same as the bandwidth of an individual diode in its transformer.

Future research on this space-power combiner technique will concentrate on (1) increasing the number of elements, (2) increasing the beam scan angle, and (3) investigating operation of the IMPATT diodes as amplifiers for a receiving array.

Appendix

THEORY FOR SINGLE-SECTION TRANSFORMER WITH IMPATT DIODE

The purpose of this Appendix is to calculate the impedance transforming properties of a single-section transformer and to derive the equations for the characteristic impedance and length of the transformer for a given diode impedance. Some comments on the IMPATT diode impedance model are also presented.

Figure A-1 shows a single-section transformer. The goal is to match the impedance Z_0 to the impedance Z_d by the correct choice of Z_T and ℓ_T. The scattering matrix for a single section of lossless transmission line is given by Reference 4.
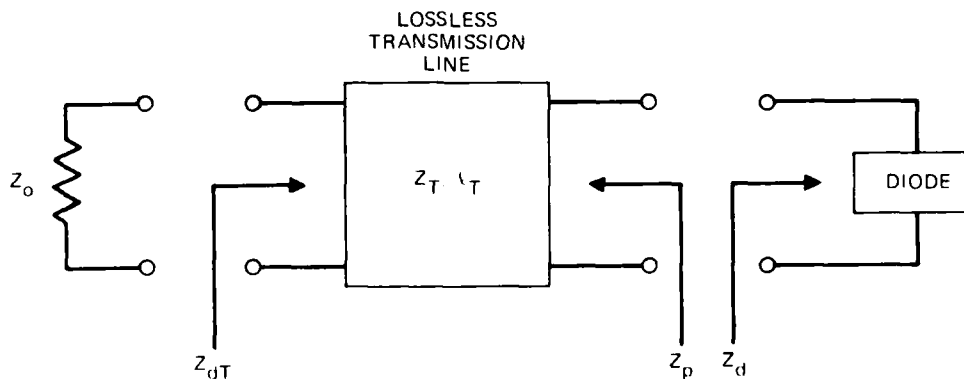
FIGURE A-1. Single-Section Transformer.

$$
\begin{bmatrix} S_{11} & S_{12} \\ \\ S_{21} & S_{22} \end{bmatrix} = \begin{bmatrix} \dfrac{r(1 - e^{-j2\beta\ell_T})}{1 - r^2 e^{-j2\beta\ell_T}} & \dfrac{(1 - r^2)e^{-j\beta\ell_T}}{1 - r^2 e^{-j2\beta\ell_T}} \\ \\ \dfrac{(1 - r^2)e^{-j\beta\ell_T}}{1 - r^2 e^{-j2\beta\ell_T}} & \dfrac{r(1 - e^{-j2\beta\ell_T})}{1 - r^2 e^{-j2\beta\ell_T}} \end{bmatrix} \qquad (A-1)
$$

31

where $r = (Z_T - Z_0)/(Z_T + Z_0)$ and $\beta = 2\pi/\lambda$. The impedance viewed by the diode at Port 2 is given by

$$Z_p = R_p + jX_p = Z_0 \left(\frac{1 + S_{22}}{1 - S_{22}} \right) \qquad (A-2)$$

Substituting from Equation A-1 gives

$$Z_p = Z_0 \left(\frac{1 - r^2 e^{-j2\beta\ell_T} + r - re^{-j2\beta\ell_T}}{1 - r^2 e^{-j2\beta\ell_T} - r + re^{-j2\beta\ell_T}} \right) \qquad (A-3)$$

Simplifying Equation A-3 and separating into resistive and reactive parts yields

$$R_p = Z_0 \frac{(1 + r)^2}{1 + 2r \cos 2\beta\ell_T + r^2} \qquad (A-4)$$

and

$$X_p = Z_0 \left(\frac{1 + r}{1 - r} \right) \frac{2r \sin 2\beta\ell_T}{1 + 2r \cos 2\beta\ell_T + r^2} \qquad (A-5)$$

We now set $R_p = R_d$ and $X_p = X_d$ and seek to invert Equations A-4 and A-5 by solving for Z_T and ℓ_T. Using the identities $\cos 2x = 1 - 2 \sin x$ and $\sin 2x = 2 \sin x \cos x$, Equations A-4 and A-5 can be rewritten, respectively, as

$$R_d = \frac{Z_0}{1 - \left(1 - \frac{Z_0^2}{Z_T^2} \right) \sin^2 \beta\ell_T} \qquad (A-6)$$

32

$$X_d = \frac{Z_T\left(1 - \frac{Z_o^2}{Z_T^2}\right)\sin \beta\ell_T \cos \beta\ell_T}{1 - \left(1 - \frac{Z_o^2}{Z_T^2}\right)\sin^2 \beta\ell_T} \qquad (A-7)$$

Solving Equation A-6 for Z_T gives

$$Z_T = Z_o\left(\frac{R_d \sin^2 \beta\ell_T}{Z_o - R_d \cos^2 \beta\ell_T}\right)^{1/2} \qquad (A-8)$$

Substituting Equation A-8 into Equation A-7, there results

$$X_d = \frac{\sqrt{R_d}\,(R_d - Z_o) \cos \beta\ell_T}{(Z_o - R_d \cos^2 \beta\ell_T)^{1/2}} \qquad (A-9)$$

Finally, solving Equation A-9 for ℓ_T gives

$$\ell_T = \frac{1}{\beta} \cos^{-1}\left(X_d\left\{\frac{Z_o}{R_d[(R_d - Z_o)^2 + X_d^2]}\right\}^{1/2}\right) \qquad (A-10)$$

Equations A-10 and A-8 are the inverted equations giving Z_T and ℓ_T in terms of the diode impedance $R_d + jX_d$.

The transformed impedance of the diode then appears at Port 1 as

$$Z_{dT} = Z_d\left(\frac{1 + S_{11}}{1 - S_{11}}\right) \qquad (A-11)$$

33

where the selected Z_T and ℓ_T are substituted into S_{11} in Equation A-1. Equation A-11 is the diode curve plotted in Figure 7. The frequency dependence of Z_{dT} is determined both by the transformer and by the frequency dependence of Z_d. We adopt a relatively simple model of an IMPATT diode having a constant negative resistance and a reactance given by

$$X_d = \frac{f_o}{f} X_o \qquad (A-12)$$

where f_o is the center frequency (10.22 gigahertz in Figure 7) and X_o is the reactance at the center frequency. In Figure A-2, we plot Equation A-11 with a Z_T and ℓ_T chosen to provide a match at a center frequency of 10.22 gigahertz. The value of X_o is a parameter. Note that across the frequency band of 10.1 to 10.6 gigahertz the transformed diode impedance is relatively insensitive to the choice of X_o.
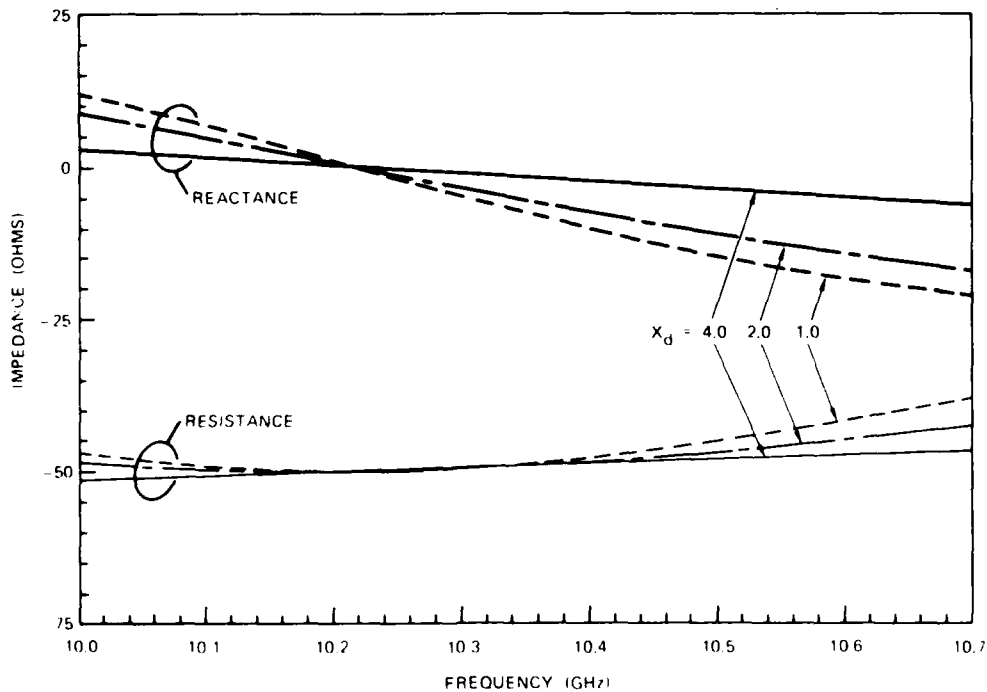
FIGURE A-2. Impedance Given by Equation A-11 Versus Frequency.

34

VI. REFERENCES

1. K. J. Russell. "Microwave Power Combining Techniques," IEEE Trans. Microwave Theory Tech., Vol. MTT-27 (1979), pp. 472-78.

2. R. J. Dinger. "Reactively Steered Adaptive Array Using Microstrip Patch Elements at 4 GHz," IEEE Trans. Antennas Propag., Vol. AP-32 (1984), pp. 848-56.

3. J. R. James, P. S. Hall, and C. Wood. Microstrip Antenna Theory and Design. London, IEE Press, 1981.

4. R. E. Collin. Foundations for Microwave Engineering. New York, McGraw-Hill, 1966.

INITIAL DISTRIBUTION

8 Naval Air Systems Command
    AIR-03D, G. Heiche (1)
    AIR-330B, F. J. Lueking (1)
    AIR-330D, C. Caposell (1)
    AIR-330E, A. Glista (1)
    AIR-330R, B. Dillon (1)
    AIR-340R, J. Smith (1)
    AIR-723 (2)
5 Chief of Naval Operations
    OP-0941 (1)
    OP-0944 (1)
    OP-098 (1)
    OP-0986 (1)
    OP-987 (1)
10 Chief of Naval Research, Arlington
    OCNR-1114
      K. Davis (1)
      D. Lewis (1)
      R. Madan (1)
      M. Morgan (1)
      J. Wright (1)
      M. Yoder (1)
    OCNR-113, A. M. Diness (1)
    OCNR-12 (1)
    OCNR-121, LCDR T. L. Swafford (1)
    OCNR-1243, CDR D. S. Siegal (1)
1 Naval Space and Warfare Command
5 Naval Sea Systems Command
    SEA-003 (1)
    SEA-09B312 (2)
    SEA-62R1
      C. E. Jedrey (1)
      T. Tasaka (1)
1 Commander in Chief, U.S. Pacific Fleet (Code 325)
1 Commander, Third Fleet, Pearl Harbor
1 Commander, Seventh Fleet, San Francisco
2 Naval Academy (Director of Research)
3 Naval Air Development Center, Warminster
    Code 4043, L. Lake (1))
    A. T. Cerino (1)
    H. H. Heffner (1)
1 Naval Ocean Systems Center, San Diego (P. Hansen)
6 Naval Research Laboratory
    Code 6800, J. Borsuk (1)
    Code 7500, J. R. Davis (1)
    Code 7550
      D. Himes (1)
      L. Wagner (1)
      W. Gabriel (1)
      C. M. Krowne (1)

END

DTIC

7-86